



# Evaluation of outdoor thermal comfort under different building external-wall-surface with different reflective directional properties using CFD analysis and model experiment

Jihui Yuan<sup>a,\*</sup>, Shingo Masuko<sup>a</sup>, Yasuhiro Shimazaki<sup>a</sup>, Toshio Yamanaka<sup>b</sup>, Tomohiro Kobayashi<sup>b</sup>

<sup>a</sup> Dept. of Architecture and Civil Eng., Graduate School of Eng., Toyohashi University of Technology, Aichi, 441-8580, Japan

<sup>b</sup> Dept. of Architectural Engineering, Graduate School of Eng., Osaka University, Osaka, 565-0871, Japan



## ARTICLE INFO

### Keywords:

Urban heat island  
Different reflective directional properties  
Building facade  
Outdoor thermal environment  
CFD analysis  
Facade-model experiment

Recently, urban heat island (UHI) has become more intense due to the increase in artificial constructions in cities. In addition, in many office buildings in big cities in Japan, except for indoor workplaces, some outdoor workplaces that surround a building are provided to improve people productivity. Therefore, a comfortable outdoor thermal environment is considered as an important topic. As one of the countermeasures for mitigating the UHI phenomenon, highly reflective (HR) materials are applied to external-wall surfaces of buildings to increase the solar reflectivity of the external-wall surface to finally reduce the heat emitted from the building external walls. These applied HR materials mainly possess diffuse HR (DHR) directional properties. In recent years, retro-reflective (RR) materials have been studied to replace the traditional DHR materials for possible application in building facades. The present study aims to use the computational-fluid-dynamics (CFD) analysis to predict the outdoor thermal environment, including air temperature ( $T_a$ ), wet-bulb globe temperature (WBGT), and standard effective temperature (SET\*) under two different building-facade types (DHR and RR properties). To further analyze the effect of DHR and RR building facades on the thermal environment, in addition to evaluating the three thermal-environment indicators ( $T_a$ , WBGT, and SET\*), this study evaluates two outdoor radiation-environment indicators, including sol-air temperature (SAT) and change operative temperature (COT) using an actual facade-model experiment. The results show that the RR building facade are more effective in reducing WBGT, SET\*, SAT, and COT.

## 1. Introduction

The well-known urban heat island (UHI) phenomenon is defined as an urban or metropolitan area that is significantly warmer than its surrounding rural areas mainly due to the modification of land surfaces and human activities. Many research works reported that the UHI phenomenon has become more serious in recent years [1–3]. The UHI effect has also been reported to increase the risk of heat-related mortality [4], increase energy consumptions of buildings for air-conditioning cooling [5], and reduce outdoor thermal comfort of human lives [6] during summer. The UHI phenomenon has been studied all over the world. In the U.S., urban areas are found to be substantially warmer than the non-urban fringe by 2.9 °C, and the average UHI amplitude is remarkably asymmetric with a 4.3 °C temperature difference during summer and only 1.3 °C during winter [7]. In the European Union, a study

reported that the UHI intensity is seasonally dependent, and the saturation is maximal in summer at approximately 3 °C and much smaller in winter [8]. In China, a research indicated that the stronger contrast between the urban and rural heat waves is associated with a greater increase in the UHI intensity in humid-climate areas such as the eastern part of China [9]. In Japan, a method was developed to separate the anthropogenically discharged heat and natural-heat radiation from the sensible heat flux and demonstrated that the sensible heat flux increased by approximately 100 W/m<sup>2</sup> during summer. The sensible heat flux at night during autumn is approximately 0 W/m<sup>2</sup> in the central part of Nagoya, Japan [10].

Alleviating the UHI phenomenon has become a very important issue worldwide. Therefore, many countermeasures have been implemented to mitigate the UHI effect [11–13]. Among the many countermeasures for alleviating the UHI phenomenon, the application of highly reflective (HR) surface materials (i.e., HR paints and HR sheet) in building facades

\* Corresponding author.

E-mail addresses: [yuan@ace.tut.ac.jp](mailto:yuan@ace.tut.ac.jp), [yuanjihui@hotmail.co.jp](mailto:yuanjihui@hotmail.co.jp) (J. Yuan).

Nomenclature	
DHR	Diffused highly reflective
RR	Retro-reflective
$T_a$	Outdoor air temperature [°C]
WBGT	Wet-bulb globe temperature [°C]
OUT_MRT	Mean radiation temperature by considering outdoor solar radiation [°C]
SET*	New standard effective temperature [°C]
RH	Relative humidity [%]
$I_g$	Global solar radiation [W/m <sup>2</sup> ]
$v$	Outdoor wind speed [m/s]
$\alpha_{cl}$	Albedo of clothed body surface [-]
$\alpha_g$	Albedo of ground surface [-]
$f_p$	Projected area ratio of human body to direct solar radiation [-]
$\beta$	Solar altitude [°]
$E_{eff}$	Effective radiation area factor [-]
$\sigma$	Stefan-Boltzmann constant [W/m <sup>2</sup> ·K <sup>4</sup> ] (=5.67 × 10 <sup>-8</sup> W/m <sup>2</sup> ·K <sup>4</sup> )
$S_{down}$	Normal direct solar radiation [W/m <sup>2</sup> ]
$D_{down}$	Diffused solar radiation [W/m <sup>2</sup> ]
$T_r$	Normal mean radiant temperature without considering solar radiation [K]
COT	Change operative temperature [°C]
SAT	Sol-air temperature [°C]
$X_r$	Coefficient from dividing the total heat-transfer coefficient by the human-body radiant heat-transfer coefficient [-]
$F_{h-f}$	View factor for viewing the facade surface from the human body [-]
$t_{sf}$	Temperature of the facade surface [°C]
$t_a$	Air temperature in the facade-model experiment [°C]
$a_h$	Solar radiation absorption of the human body [-]
$\alpha_h$	Human-body total heat-transfer coefficient [W/m <sup>2</sup> ·K]
$R_{fl}$	Downward solar radiation reflection from facade [W/m <sup>2</sup> ]

and roofs have been widely implemented as an accepted solution for building energy savings and UHI mitigation [14]. Compared with the normal building-surface materials with smaller solar reflectance, HR materials are considered to largely reflect the incident solar radiation of a building surface. Hence, they can reduce the absorption of solar radiation by the external walls. Therefore, many HR materials have been developed and studied and developed for application to building surfaces and pavements. Among them are pavement materials used in outdoor environment for UHI mitigation [15], smart HR paints applied to building facades to mitigate the UHI phenomenon and minimize energy consumption of buildings [16], and HR coating materials applied to residential buildings in California and Florida, which contribute to cooling energy savings of approximately 10%–70% [17].

Most HR materials are diffused HR (DHR) materials. Studies have shown that if DHR materials are used on building facades, the solar radiation incident to the building-wall surface is reflected to and subsequently absorbed by the adjacent building-wall surfaces or roads. Thus, the solar radiant heat remains in the urban canyon [18]. To better mitigate the UHI phenomenon and replace the DHR materials applied to building facades, retro-reflective (RR) materials have been developed and studied owing to their advantage of being able to reflect the incident solar radiation to the sky without being absorbed by nearby buildings or roads [19–23].

Similar to DHR materials, optical experiments and simulation research on the advantage of RR materials in mitigating the UHI phenomenon have also been widely conducted. A study proposed a type of RR film, which possesses a RR property and a wavelength-selection property, while having the same degree of transparency as that of transparent glass, for used in building windows. The measurement results showed that this RR window film increased the ratio of upward reflection, thereby mitigating the UHI effect [24]. A simulation study used a numerical model to predict the upward-to-downward reflection ratio of glass-bead RR material, which has a refractive index of 1.9, and almost the same long-wavelength emissivity and short-wavelength reflectance as the other glass materials, under different incidents of solar radiation. The results demonstrated that the upward reflective ratio of the glass-bead RR materials at a small solar altitude was larger than that at a large solar altitude [25]. An experimental and analytical study was carried out to predict the angular reflectance of RR films. The ad hoc experiment found that an evident tendency to reflect the incident

radiation much more backward to the direction of the source, and the increase of the incident angle produces a remarkable decrease of the reflectance capability of these RR films. The analytical study revealed that RR films could be applied to urban-building coatings and pavements beyond the urban canyon to effectively mitigate the UHI effect [26]. However, some studies have shown that RR materials will lose their RR performance when the incident angle of sunlight on a surface exceeded an angle of approximately 50° with respect to the wall-surface normal [27,28].

The effects of orientations, aspect ratios, and coating materials of urban blocks on the outdoor thermal environment have been studied. The influence of orientations and aspect ratios of urban buildings, pavement materials, and vegetation on the thermal stress was analyzed using ENVI-met [29]. The effect of DHR building facades and greening rate on the local microclimate of a city was predicted using the computational-fluid-dynamics (CFD) analysis method [30].

Nevertheless, only a few studies have used the CFD-analysis method to assess the effect of RR building envelopes on the urban outdoor thermal environment. Thus, the present study uses the CFD-analysis method to evaluate the outdoor thermal environment, including air temperature (Ta), wet-bulb globe temperature (WBGT), and new standard effective temperature (SET\*), under three different reflective directional building facades (DHR, SR, and RR) conditions. To further analyze in detail the effect of DHR and RR building facades on the thermal environment, in addition to the three outdoor thermal-environment indicators (Ta, WBGT, and SET\*), this study conducts an actual facade-model experiment with DHR and RR facades to evaluate the outdoor radiation-environment indicators. These indicators include the sol-air temperature (SAT) and change operative temperature (COT) from different reflective directional building facades (DHR and RR).

## 2. Materials and methods

This study uses the methods of CFD analysis and actual facade-model measurement to achieve the research objective. CFD analyzes three outdoor thermal-environment indexes (Ta, WBGT, and SET\*) under two different reflective directional building facades (DHR and RR). The actual facade-model experiment is conducted to further analyze in detail the influence of DHR and RR building facades on the outdoor thermal environment, which includes Ta, WBGT, and SET\*, and on two outdoor

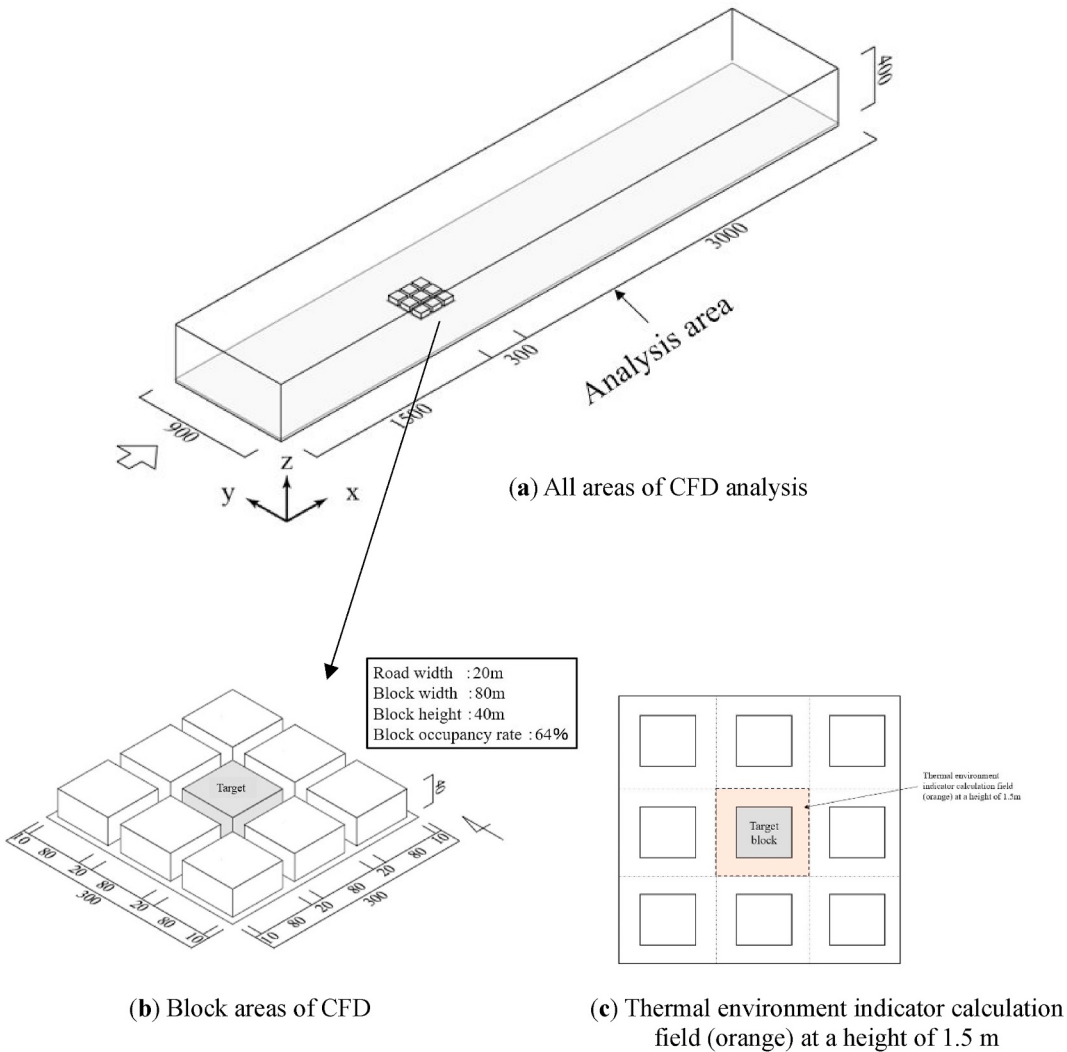


Fig. 1. Analysis domain and target blocks.

radiation-environment indicators (SAT and COT) from different reflective directional building facades.

The CFD analysis is introduced in Section 2.1, and the actual facade-model experiment is introduced in Section 2.3.

## 2.1. CFD simulation

### 2.1.1. Analysis domain

Fig. 1 shows the analysis domain, which is set to 4800 m (X-axis direction)  $\times$  900 m (Y-axis direction)  $\times$  400 m (Z-axis direction). The size of the blocks is 300 m  $\times$  300 m  $\times$  40 m. The size of each block is set to 80 m  $\times$  80 m  $\times$  40 m, the road width is set to 20 m, and the block occupancy rate is set to 64% according to Ref. [31]. The analyzed blocks are located in Osaka City, Japan (34.4°N, 135.3°E).

### 2.1.2. Analysis conditions and case

Similar to the CFD software “ANSYS Fluent”, which is often used worldwide, this study uses the STREAM software (<https://www.cradle.co.jp/>), which is often used in Japan [32]. The conditions set in the CFD analysis are listed in detail in Table 1. The turbulence model “Standard k- $\epsilon$  (SKE) model” and a normal structure grid-mesh type (where the

number of mesh is 1,369,368) are adopted in the CFD analysis. Indoor  $T_a$  of the block buildings is set to 24 °C for cooling. For the input meteorological parameters, initial inflow  $T_a$  is set to 30.6 °C, the wind speed is set to 3.0 m/s (at a horizontal elevation of 28 m), the wind direction is set to west, and the direct and diffused solar radiations at the actual local time on June 21, 2020 are based on the weather database in Osaka. The building external-wall structure from indoor to outdoor is made of plywood, foam polystyrene, concrete and mortar. Its thermal transmittance is calculated and set to 0.90 W/m<sup>2</sup>·K. The ground is made of asphalt and organic soil, and the internal temperature of the ground is set to a fixed value of 15 °C. In addition, for the short-wavelength solar reflectance, the ground surface is set to a constant value of 0.25. The exterior envelopes, including the rooftop and exterior walls of the urban canyon, are set to a constant value of 0.5 except for the target block. The building facades of the target block are set to a constant value of 0.7 (based on the measured solar reflectance of an RR sample detailed in Section 2.2) with different reflective directional properties (DHR and RR). For the long-wavelength emissivity, all surfaces of the urban blocks and ground are set to a constant value of 0.9 in this study.

For the CFD-analysis cases, Fig. 2 shows that two types of building facades (DHR and RR) with fixed solar reflectance of 0.7 are designed for

**Table 1**

Analysis conditions of the CFD simulation.

CFD code	STREAM V14 RC2
Turbulence model	Standard k-ε model, 1-h steady-state analysis performed using radiation view factor method with consideration of solar radiation
Algorithm	SIMPLER
Discretization scheme	QUICK
Boundary condition	X <sub>min</sub> Fixed temperature, Free slip X <sub>max</sub> Natural outflow Y <sub>min</sub> Fixed temperature, Free slip Y <sub>max</sub> Fixed temperature, Free slip Z <sub>min</sub> Fixed temperature, Free slip Z <sub>max</sub> Fixed temperature, Free slip Fluid-Wall surface Temperature power law, No slip $\left(\frac{u}{u^*} = \frac{u^*y}{v} = Y + \right) \cong 11.4$ Fluid-Ground surface Temperature power law Exponent reciprocal (n = 4)
Initial temperature of inflow	30.6 °C on June 21st
Direct and diffused solar radiation	According to the meteorological database at the actual time in Osaka, Japan
Wind speed	3.0 m/s at a horizontal elevation of 28 m (based on meteorological database of Osaka, Japan)
Wind direction	West
Thermal transmittance of external-wall structure	0.94W/m <sup>2</sup> K
Short-wavelength solar reflectance & long-wavelength emissivity	<input type="checkbox"/> Short-wavelength solar reflectance: - Constant value of 0.25 for ground surface (asphalt); - Constant value of 0.5 for exterior envelopes (rooftop and exterior walls except for target block of urban canyon); - Constant value of 0.7 for building facades of target block; <input type="checkbox"/> Long-wavelength emissivity: - Constant value of 0.9 for all surfaces of urban blocks including ground ● DHR facade (at local time 10:00, 12:00, and 15:00) ● RR facade (at local time 10:00, 12:00, and 15:00)
Analysis cases	Number: 1,369,368 (247 × 132 × 42) Mesh type: structured grid
Mesh	
Cycle	5000

the target block in the CFD simulation. Additionally, the CFD analysis is conducted at local times of 10:00, 12:00, and 15:00 on June 21, 2020.

### 2.1.3. Outdoor thermal environment indicators in CFD simulation

This study adopts three main outdoor thermal-environment indicators often used in Japan [33], including one microclimate condition ( $T_a$ ), and two outdoor thermal-comfort conditions (WBGT and SET\*), to evaluate the outdoor thermal environment under two cases of DHR and RR building facades.

Outdoor thermal-comfort indicator “WBGT” is improved by considering the outdoor global solar radiation [34] based on the International Organization for Standardization [35]. The improved WBGT used in this study is derived using Eq. (1).

$$\text{WBGT} = 0.735T_a + 0.0374\text{RH} + 0.00292(T_a \text{ RH}) + 7.619I_g - 4.557I_g^2 - 0.0572v - 4.064 \quad (1)$$

where “ $T_a$ ” is the outdoor  $T_a$  [°C], “RH” is the relative humidity [%] (an initial value of 68% is set in this study), “ $I_g$ ” is the global solar radiation [W/m<sup>2</sup>], and “ $v$ ” is the outdoor wind speed [m/s].

The other outdoor thermal-comfort indicator, i.e., “SET\*” is calculated by considering the outdoor mean radiant temperature (abbreviated as OUT\_MRT), which is calculated by considering the outdoor solar radiation proposed in Ref. [36]. OUT\_MRT can be derived using Eqs. (2) and (3).

$$\text{OUT\_MRT} = \left[ \left( \frac{f_n(1 - \alpha_{cl})S_{down}}{E_{eff}\delta} \right) + \frac{1}{\delta}(1 - \alpha_{cl})\{D_{down} + (D_{down} + S_{down})\alpha_g\} + T_r^4 \right]^{0.25} \quad (2)$$

$$f_p = 0.42\cos\beta + 0.043\sin\beta \quad (3)$$

where “ $\alpha_{cl}$ ” is the albedo of a clothed body surface [—] (here, it is set to 0.4). “ $\alpha_g$ ” is the albedo of the ground surface [—] (here, it is set to 0.75). “ $f_p$ ” is the projected area ratio of the human body to direct solar radiation [—], “ $\beta$ ” is the solar altitude [°], and “ $E_{eff}$ ” is the effective radiation-area factor [—] (here, it is set to 0.75). “ $\sigma$ ” is the Stefan-Boltzmann constant [W/m<sup>2</sup>·K<sup>4</sup>] ( $5.67 \times 10^{-8}$  [W/m<sup>2</sup>·K<sup>4</sup>]), “ $S_{down}$ ” is the normal direct solar radiation [W/m<sup>2</sup>], “ $D_{down}$ ” is the diffused solar radiation [W/m<sup>2</sup>], and “ $T_r$ ” is the normal mean radiant temperature that does not consider the solar radiation [K].

In this study, CFD simulation SET\* is derived using the following: the total body mass of 62 kg, body core temperature of 36.6 °C, met value of human dress of 0.2 clo, metabolic-heat production of 1.0 met (approximately 58.2 W/m<sup>2</sup>), heat of vaporized water that diffuses through the skin layer of 3.94 W/m<sup>2</sup>, and minimum skin-heat conductance of 6.3 W/m<sup>2</sup>.

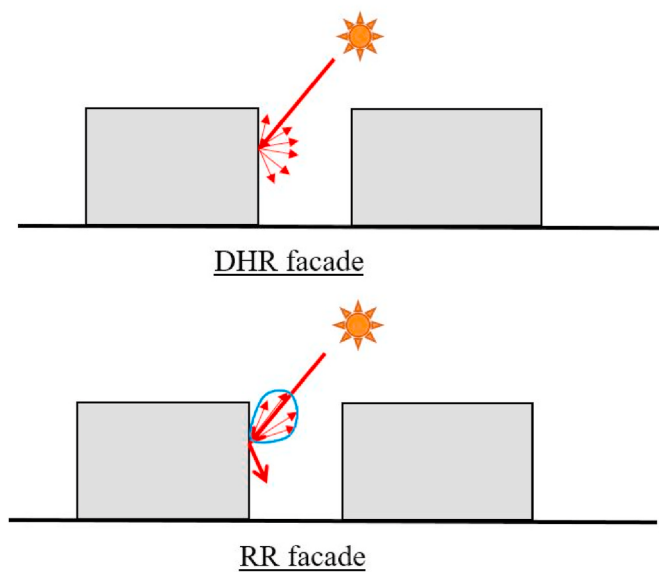


**Fig. 2.** Building facades with two different reflection directional properties (DHR and RR).

## 2.2. RR sample and laboratory optical measurement

**Fig. 3(a)** and **3(b)** show that a type of prism RR sample is chosen for the optical measurement in this study. The measured solar absorptivity,

diffused solar reflectivity, specular reflectivity, and retro-reflectivity of the prism RR sample under different incident-light angles using an optical apparatus [as shown in **Fig. 3(c)**], which is developed by our laboratory, are shown in **Fig. 4**.

Next, the measured reflection properties (solar absorptivity, diffused solar reflectivity, specular reflectivity, and retro-reflectivity) of the prism RR sample are set for the external-wall-surface materials of the target block used in the CFD simulation.

### 2.3. Actual facade-model experiment

Three outdoor thermal-environment indicators ( $T_a$ , WBGT, and SET\*) and two outdoor radiation-environment indexes (SAT and COT) near the building facade are adopted in the actual facade-model experiment to analyze in more detail the effect of different reflective directional facades on the outdoor thermal environment.

#### 2.3.1. Facade-model experimental setup

To further investigate the outdoor radiation environment from two different reflective directional building facades, namely, DHR and RR, as shown in **Fig. 5**, two full-scale facade surface with a prism RR material and an ivory DHR material are built in this actual facade-model experiment.

The global solar reflectance of the prism RR and traditional ivory DHR samples is measured according to the JIS K5602 standard [37]. The results are listed in **Table 2**. The global solar reflectance of both samples exceeds 0.7 (0.72 for the prism RR sample and 0.71 for the ivory DHR sample).

The instruments used to derive the outdoor thermal-environment indicators ( $T_a$ , WBGT, and SET\*) and outdoor radiation-environment

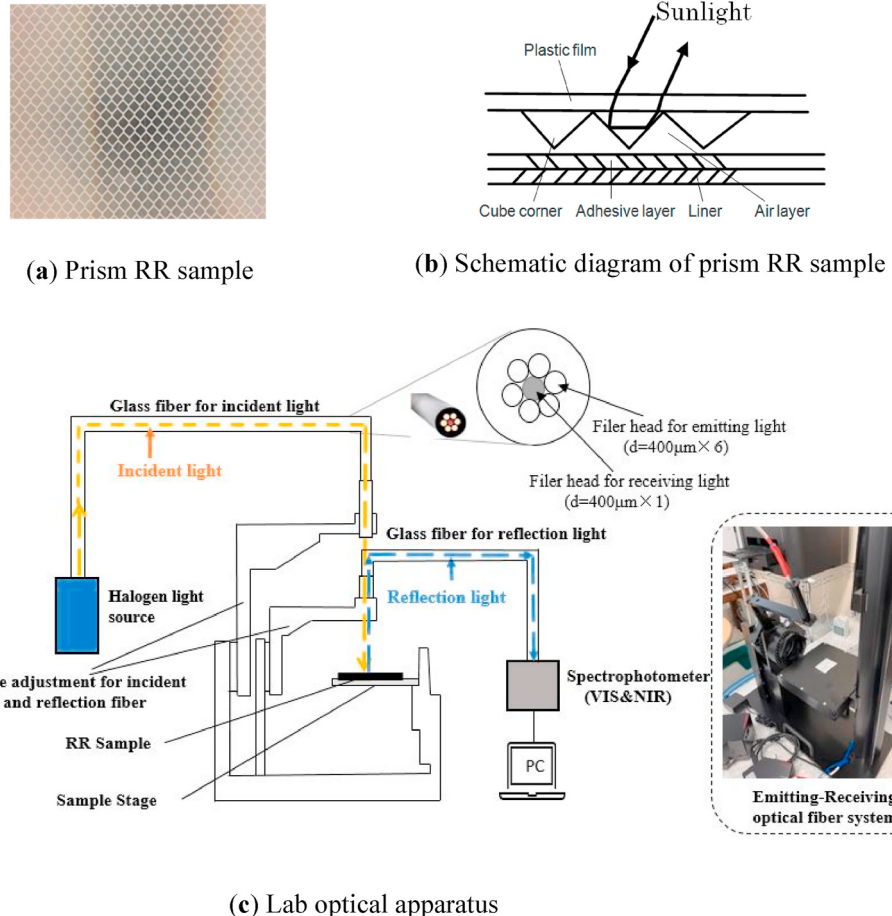


**Fig. 3.** (a) Prism RR sample. (b) Schematic diagram of the prism RR sample. (c) Laboratory optical apparatus.

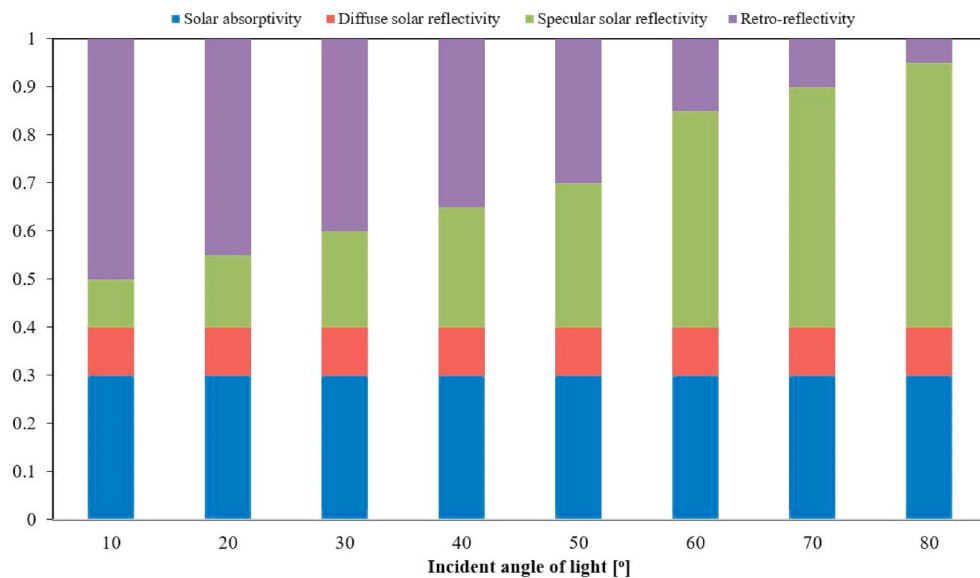


**Fig. 4.** Measured solar absorptivity, diffused solar reflectivity, specular reflectivity and retro-reflectivity of the prism RR sample under different angles of the incident light.

indicators (SAT and COT) in the experiment are detailed as follows:

- T-type thermocouple: temperature range ( $-40^{\circ}\text{C}$  to  $+125^{\circ}\text{C}$ ) with a deviation of  $\pm 0.5^{\circ}\text{C}$
- Pyranometer: measurement wavelength range (400–1100 nm); measured solar-irradiance range ( $0$ – $2000 \text{ W/m}^2$  with a deviation of  $\pm 50 \text{ W/m}^2$ ); accuracy of the guaranteed temperature range (from  $-30^{\circ}\text{C}$  to  $+70^{\circ}\text{C}$ )
- Thermometer: temperature range ( $-25^{\circ}\text{C}$  to  $+70^{\circ}\text{C}$  with a deviation of  $\pm 0.3^{\circ}\text{C}$ ); relative humidity range (0–99% with a deviation of  $\pm 2.5\%$ )
- Black globe: diameter 150 mm; temperature range ( $0^{\circ}\text{C}$ – $100^{\circ}\text{C}$  with a deviation of  $\pm 0.5^{\circ}\text{C}$ )
- Three-dimensional wind-direction anemometer: wind speed range (0–60 m/s with accuracy of  $3\% \pm 0.05 \text{ m/s}$  of the reading value); wind-direction range (0– $540^{\circ}$  with a deviation of  $\pm 3^{\circ}$ ).

The experiment was performed in Toyohashi City, Japan ( $34.7^{\circ}\text{N}$ ,  $137.4^{\circ}\text{E}$ ) during a sunny day on August 29, 2021 from 10:00 to 16:00. The urban aspect ratio (facade height:  $H$ /distance between two facades:  $D$ ) was set to 1.5.

### 2.3.2. Outdoor radiation-environment indicator

In addition to the three outdoor thermal-environment indicators ( $T_a$ , WBGT, and SET\*), the actual facade-model experiment added two outdoor radiation-environment indicators (SAT and COT) to further investigate the outdoor radiation environment from different reflective directional building facades (DHR and RR).

To quantitatively identify the thermal effect of the amount of downward-reflected solar radiation from the facade surface on a nearby outdoor radiant environment, as shown in Fig. 5, SAT meters with direct solar-radiation shielding are developed and installed near the prism RR and ivory DHR facades. The equivalent outside  $T_a$  is measured. The SAT meter is manufactured based on the standards of the Building Materials Testing Center [38], and a T-type thermocouple is embedded between the blackbody-treated copper plate and heat-insulating material, and they are closely attached.

Outdoor radiation-environment indicator “COT” consists of a short-wavelength component to address the amount of downward solar-radiation reflection from the facade surface and the long-wavelength component due to the surface temperature of the façade. It

quantitatively indicates the effect of the facade surface on the warmth of a human body. It can be derived using Eq. (4) [39].

$$COT = X_r * F_{h-f} * (t_{sf} - t_a) + \left( \frac{a_h}{\alpha_h} \right) * f_p * R_{f\downarrow} \quad (4)$$

where “ $X_r$ ” is the coefficient from the division of the total heat-transfer coefficient by the human-body radiant heat-transfer coefficient (here, it is set to 0.5) [–]. “ $F_{h-f}$ ” is the view factor for viewing the facade surface from the human body (=0.5) [–]. “ $t_{sf}$ ” is the temperature of the facade surface [ $^{\circ}\text{C}$ ]. “ $t_a$ ” is the  $T_a$  [ $^{\circ}\text{C}$ ]. “ $a_h$ ” is the solar-radiation absorption of a human-body (here, it is set to 0.6) [–]. “ $\alpha_h$ ” is the human-body total heat-transfer coefficient (here, it is set to  $11.0 \text{ W/m}^2\cdot\text{K}$ ). “ $R_{f\downarrow}$ ” is the downward solar-radiation reflection from the facade [ $\text{W/m}^2$ ], and “ $f_p$ ” is the projected area ratio of the human body to direct solar radiation [–] [the same as that in Eq. (3)].

## 3. Results

### 3.1. Comparison of the outdoor thermal-environment indicators using CFD

$T_a$ , WBGT, and SET\* at a height of 1.5 m in the orange area near the target block [as shown in Fig. 1(c)] are evaluated using CFD analysis at different local times (JST 10:00, 12:00, and 15:00 on June 21, 2020) under two different reflective directional building facades.

The result of outdoor  $T_a$  is shown in Fig. 6(a). Fig. 6(a) shows that  $T_a$  under the RR facade condition is almost the same as that under the DHR facade condition. It is only approximately  $0.03^{\circ}\text{C}$  (0.09%) higher at 10:00, approximately  $0.06^{\circ}\text{C}$  (0.19%) higher at 12:00, and approximately  $0.04^{\circ}\text{C}$  (0.13%) higher at 15:00. The prediction results also show that in the three time periods,  $T_a$  at 12:00 is the highest regardless of the considered reflective directional building facades.

The result of outdoor WBGT is shown in Fig. 6(b). Compared with that under the DHR facade condition, Fig. 6(b) shows that indicator WBGT under the RR facade condition indicates almost no difference at 10:00, which shows only a slight difference of approximately  $0.01^{\circ}\text{C}$  (0.03%). However, the results show that the WBGT indicator under the RR building-facade condition is lower than that under the DHR building-facade condition, approximately  $1.2^{\circ}\text{C}$  (3.74%) lower at 12:00 and approximately  $0.6^{\circ}\text{C}$  (1.81%) lower at 15:00. The prediction results also

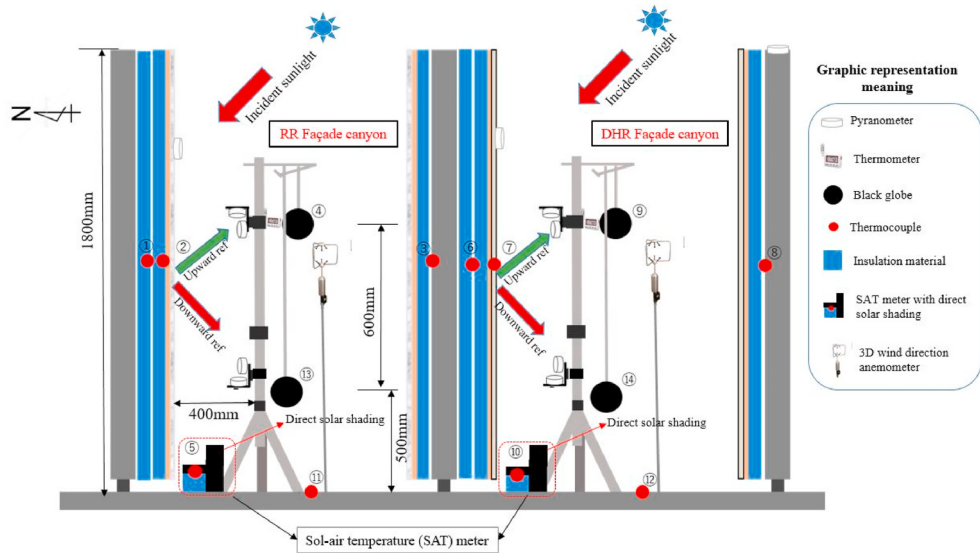


**Fig. 5.** Facade-model experimental setup.

**Table 2**  
Measured global solar reflectance of two samples used in the experiment.

Sample	Global solar reflectance [-]
Prism RR sheet	0.72
Traditional ivory DHR plate	0.71

show that in the three time periods, WBGT at 12:00 is the highest regardless of the considered reflective directional building facades.

The result of outdoor thermal-environment indicator SET\* is shown in Fig. 6(c), which shows that SET\* under the RR building facade is lower than that under the DHR building facade, which is approximately 0.2 °C (0.52%) lower at 10:00, approximately 0.5 °C (1.36%) lower at

12:00, and approximately 0.2 °C (0.51%) lower at 15:00. Similar to the results of the  $T_a$  and WBGT indicators, the SET\* indicator also shows that in the three time periods, SET\* at 12:00 is the highest regardless of the considered reflective directional building facades.

### 3.2. Comparison of $T_a$ , WBGT, and SET\* using facade-model experiment

According to the CFD simulation evaluation, the three outdoor thermal-environment indicators ( $T_a$ , WBGT, and SET\*) are also measured and evaluated using the facade-model experiment implemented on a sunny day, August 29, 2021, from 10:00 to 16:00.

The outdoor  $T_a$  indicator is measured from 10:00 to 16:00 at a 1-min interval using a thermometer (detailed in Section 2.3.1), which is placed 1.1 m above the ground and 0.4 m from the left facade (as shown in Fig. 5). The hourly  $T_a$  under the two building-facade cases (DHR and RR) is calculated and shown in Fig. 7(a). Compared with that under the DHR facade condition, the approximate outdoor  $T_a$  values under the RR facade condition are approximately 1.1 °C (3.20%) higher at 10:00, 0.14 °C (0.40%) higher at 11:00, 0.13 °C (0.33%) lower at 12:00, 0.26 °C (0.70%) lower at 13:00, 0.22 °C (0.57%) lower at 14:00, 0.03 °C (0.07%) higher at 15:00, and 0.06 °C (0.17%) higher at 16:00. In general, except for the 1.1 °C (3.20%) difference at 10:00, the difference in the  $T_a$

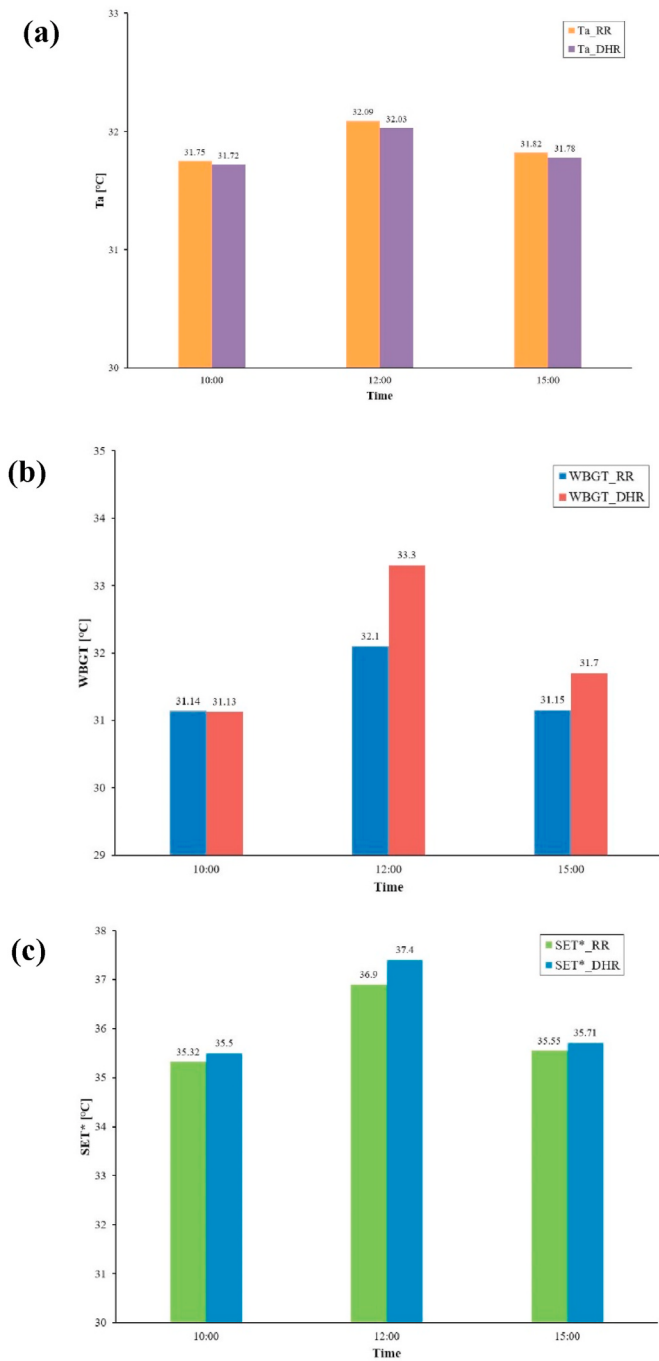


**Fig. 6.**  $T_a$ , WBGT and  $SET^*$  at a height of 1.5 m at different local times (10:00, 12:00, and 15:00) under two different reflective directional facades (DHR and RR) evaluated using CFD.

indicator for the remaining times is not large, which is only approximately  $0.06\text{ }^\circ\text{C}$  (0.17%), on average. In addition, the results show that during noontime when the sun elevation angle is the largest, the  $T_a$  indicator under the RR facade condition is approximately  $0.2\text{ }^\circ\text{C}$  (0.53%) lower on average than that under the DHR facade condition.

The hourly WBGT indicator under the two cases of building facades (DHR and RR) is calculated and shown in Fig. 7(b). Compared with that under the DHR facade condition, Fig. 7(c) shows that the approximate WBGT values under the RR facade condition are only approximately  $0.1\text{ }^\circ\text{C}$  (0.40%) higher at 10:00,  $1.6\text{ }^\circ\text{C}$  (5.10%) lower at 11:00,  $1.9\text{ }^\circ\text{C}$  (6.03%) lower at 12:00,  $1.2\text{ }^\circ\text{C}$  (3.74%) lower at 13:00,  $1.1\text{ }^\circ\text{C}$  (3.48%) lower at 14:00,  $0.6\text{ }^\circ\text{C}$  (1.99%) lower at 15:00, and  $0.7\text{ }^\circ\text{C}$  (2.27%) lower

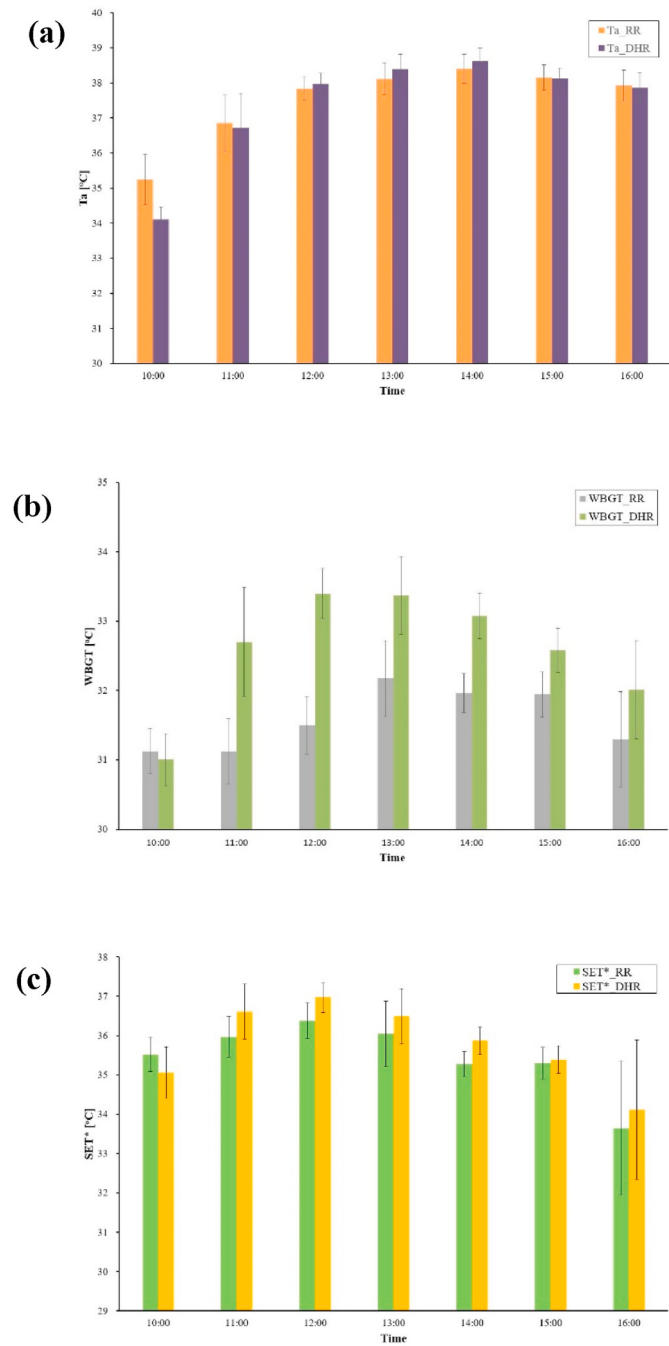


**Fig. 7.** Hourly  $T_a$ , WBGT, and  $SET^*$  at a height of 1.1 m from 10:00 to 16:00 under two different reflective directional facades (DHR and RR) evaluated using the facade-model experiment.

at 16:00. In general, compared with that under the DHR facade condition, except for the approximately  $0.1\text{ }^\circ\text{C}$  (0.40%) higher value (almost no difference) at 10:00, the RR facade condition can reduce WBGT by an average of approximately  $1.2\text{ }^\circ\text{C}$  (3.75%) at other times (11:00 to 16:00). In particular, at noon when the sun elevation angle is the largest, the reduction shows a maximum value of approximately  $1.9\text{ }^\circ\text{C}$  (6.03%).

The hourly  $SET^*$  under the two cases of building facades (DHR and RR) is calculated and shown in Fig. 7(c). Compared with that under the DHR facade condition, Fig. 7(c) shows that the approximate  $SET^*$  values under the RR facade condition is only approximately  $0.4\text{ }^\circ\text{C}$  (1.30%) higher at 10:00,  $0.6\text{ }^\circ\text{C}$  (1.78%) lower at 11:00,  $0.6\text{ }^\circ\text{C}$  (1.60%) lower at 12:00,  $0.4\text{ }^\circ\text{C}$  (1.21%) lower at 13:00,  $0.6\text{ }^\circ\text{C}$  (1.70%) lower at 14:00,

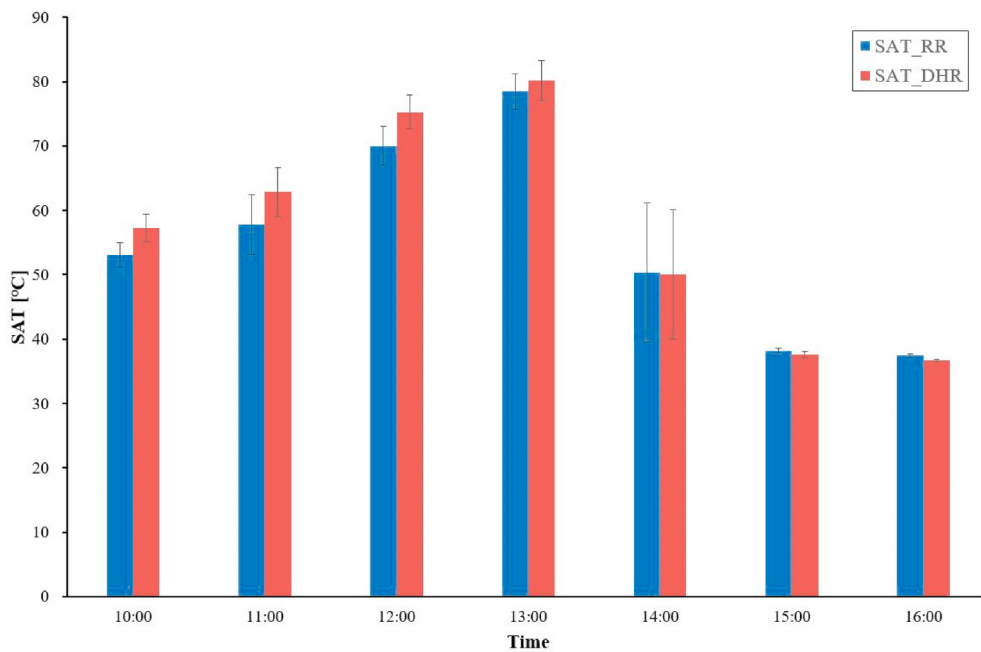


**Fig. 8.** Hourly SAT measured from 10:00 to 16:00 under two different reflective directional facades (DHR and RR) evaluated using the facade-model experiment.

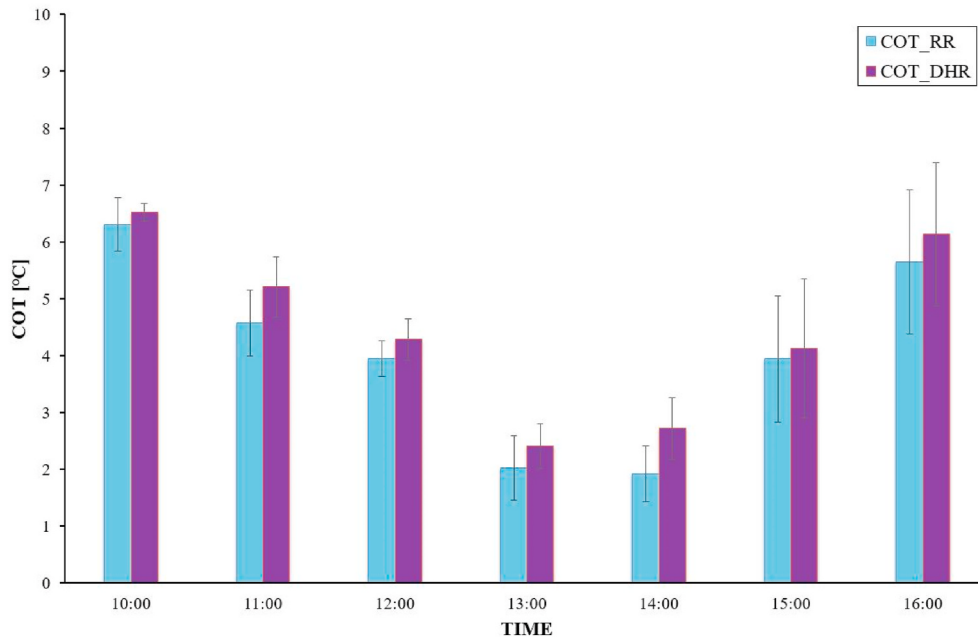


**Fig. 9.** Hourly COT measured from 10:00 to 16:00 under two different reflective directional facades (DHR and RR) evaluated using the facade-model experiment.

0.1 °C (0.25%) lower at 15:00, and 0.5 °C (1.40%) lower at 16:00. Similar to the WBGT result, the RR facade condition can reduce the SET\* value by an average of approximately 0.55 °C (1.57%), and the reduction effect of SET\* is more significant at noontime when the sun elevation angle is the largest.

### 3.3. Comparison of SAT and COT using facade-model experiment

Fig. 5 shows that two SAT meters with direct solar-radiation shielding are developed and installed near the RR and DHR facades to quantitatively evaluate the thermal effect of the amount of downward-reflected solar radiation from the facade surface in an outdoor radiant environment. SAT is measured from 10:00 to 16:00 at a 1-min interval,

and the hourly SAT values under the two conditions of RR and DHR facades are calculated and shown in Fig. 8.

The results show that the approximate SAT indicator values under the RR facade condition are approximately 4.3 °C (7.99%) lower at 10:00, 5.1 °C (8.70%) lower at 11:00, 5.3 °C (7.51%) lower at 12:00, 1.8 °C (2.26%) lower at 13:00, and an average of approximately 0.5 °C (1.29%) higher (almost no large difference) from 14:00 to 16:00 compared with those under the DHR facade condition.

The COT indicator under the two conditions of RR and DHR facades is derived using Eq. (4). The hourly COT values under the RR and DHR facade conditions are calculated and shown in Fig. 9.

The results show that the approximate COT values under the RR facade condition are lower than those under the DHR facade condition at

all time periods (10:00 to 16:00). These are 0.2 °C (3.32%) lower at 10:00, 0.6 °C (13.88%) lower at 11:00, 0.4 °C (8.69%) lower at 12:00, 0.4 °C (18.67%) lower at 13:00, 0.8 °C (41.60%) lower at 14:00, 0.2 °C (4.63%) lower at 15:00, and 0.5 °C (8.66%) lower at 16:00. The results also show that regardless of whether RR or DHR facade is considered, the COT indicator shows a downward trend from 10:00 to 13:00 and an upward trend from 13:00 to 16:00.

#### 4. Discussion and limitations

The comparison results of outdoor  $T_a$  evaluated using the CFD simulation under two different reflection directional building facades (DHR and RR) reveal that the  $T_a$  difference at three time periods (10:00, 12:00, and 15:00) under the DHR and RR facade cases is very small, and the average  $T_a$  difference under the two building facades is only approximately 0.04 °C (0.14%). In addition, the results of the actual facade-model experiment also show a  $T_a$  difference of only 0.06 °C (0.17%) on average from 11:00 to 16:00 under the DHR and RR facade conditions. Thus, we consider that the DHR and RR facades with almost the same solar reflectance have little effect on outdoor  $T_a$ .

However, comparison of the outdoor thermal-environment indicator WBGT under the two DHR and RR facades cases evaluated using the CFD simulation reveals that the difference in WBGT is approximately 0.7 °C (2.75%) ( $WBGT_{DHR} > WBGT_{RR}$ ) on average, except at 10:00 when no difference is observed. Additionally, WBGT evaluated using the actual facade-model experiment shows a large difference of approximately 1.2 °C (3.75%) ( $WBGT_{DHR} > WBGT_{RR}$ ) on average, especially at noon when the sun elevation angle is the largest. The difference in WBGT shows a maximum value of approximately 1.9 °C (6.03%) ( $WBGT_{DHR} > WBGT_{RR}$ ). Thus, we can conclude that the different reflective directional facades (DHR and RR) at almost the same solar reflectance exert a relatively greater effect on outdoor thermal-environment indicator WBGT, and we consider that the RR building facade is more effective in reducing the WBGT than the DHR building facade.

The comparison results of outdoor thermal-environment indicator SET\* by considering OUT\_MRT under the DHR and RR facade cases evaluated using the CFD simulation show that the difference in SET\* is approximately 0.3 °C (0.78%) ( $SET^*_{DHR} > SET^*_{RR}$ ) on average. The SET\* difference at noon (12:00) is the largest, which is approximately 0.5 °C (1.36%) ( $SET^*_{DHR} > SET^*_{RR}$ ). In addition, the difference in SET\* evaluated using the actual facade-model experiment shows a difference of approximately 0.55 °C (1.57%) ( $SET^*_{DHR} > SET^*_{RR}$ ) on average. The relatively larger reduction effect in SET\* occurs during noontime when the sun elevation angle is the largest. Therefore, we can conclude that similar to WBGT, the RR building facade is more effective in reducing the SET\*, when the DHR and RR facade surfaces have almost the same solar reflectance.

When WBGT and SET\* are calculated, the incident solar radiation reflected from the building facades is considered because RR building facades have a special reflective directional property that can reflect the incident solar radiation to the sky. Therefore, the environment can greatly reduce the reflection from the RR building facade, which is considered as the main reason for the reduction in WBGT and SET\*. This effect is also consistent with the conclusion of another study [40] that demonstrated that RR walls could increase the amount of solar radiation incident on the wall surface reflected to the sky, thereby reducing the amount of solar radiation diffusively reflected by the wall to the environment compared with DHR walls.

The comparison of outdoor radiation-environment indicator SAT between the DHR and RR facades shows an average difference of approximately 2.1 °C (3.81%) ( $SAT_{DHR} > SAT_{RR}$ ) from 10:00 to 16:00, especially during noontime. SAT under the RR facade condition is approximately 5.3 °C (7.51%) lower than that under the DHR facade condition. The difference in COT between the DHR and RR facade conditions is approximately 0.5 °C (10.71%) ( $COT_{DHR} > COT_{RR}$ ) on average from 10:00 to 16:00. We conclude that the RR facade can

relatively reduce the COT compared with the DHR facade. The reason is that the amount of downward solar radiation reflected from the RR facade is less than that from the DHR facade. Therefore, we consider that the RR facade can contribute to the reduction in SAT and COT owing to the special reflective directional property of RR materials.

The results of SAT and COT are almost consistent with the experimental research result on RR window films [41], which demonstrated that the RR window film could reduce SAT by approximately 3.0 °C on average from 12:00 to 15:00. It also reduced COT by approximately 2.0 °C at 11:50 on August 16, 2012 in Tokyo, Japan, compared with the normal low-E window film.

Through the abovementioned analysis and discussion of the results, we can conclude that RR building facades with the same solar reflectance as the DHR facades can effectively reduce the outdoor thermal- and radiation-environment indicators, including WBGT, SET\*, SAT, and COT. Thus, they can potentially improve the outdoor environment and minimize the UHI phenomenon.

The limitations of this study are mainly summarized in the following aspects. First, this study only adopted the three most common thermal-environment indicators ( $T_a$ , WBGT, and SET\*) for analysis, although many outdoor thermal-environment indicators should be involved in the research [42]. Second, the CFD analysis was limited to one city (Osaka, Japan) and one representative day, and the influence of other surrounding factors such as greenery and wind direction were ignored in this study. Third, the facade size used in the actual facade-model experiment was slightly small (height: 1.8 m × width: 1.5 m) and needs to be increased in future experiments.

In addition, although this study used the CFD analysis and actual experimental methods to prove the advantages of RR facades compared with DHR facades, some studies pointed out some disadvantages of the DHR materials used in an urban canyon. A study found that DHR surfaces might lead to reduction in surrounding wind speeds and vertical mixing and lower the planetary boundary-layer height. Thus, it poses negative effect in the reduction in ventilation associated with surface cooling [43]. Another study found that DHR surfaces could cause stagnation of air near the surface, which could potentially impede the dilution or dispersion of pollutants and cause degraded air quality in urban areas [44]. From the aforementioned research conclusions, we can observe that whether RR materials bring the same negative effects must be profoundly studied, and similar investigations should be implemented in future research.

#### 5. Conclusions and future work

This study used the CFD simulation to predict the three common outdoor thermal-environment indicators, namely,  $T_a$ , WBGT, and SET\*, by considering the different reflective directional properties of building facades (DHR and RR). To set the reflective directional properties of a prism RR material in the exterior wall surface simulated by CFD, the optical apparatus developed by our laboratory was used to determine the properties of the prism RR sample. After understanding the reflective directional properties of the RR materials, we introduced a DHR material with almost the same solar reflectance as the prism RR material and RR on the facade surface in the CFD simulation. We then installed it on a representative city and selected a representative day to analyze the effect of different reflective directional building facades (DHR and RR) on the urban outdoor thermal environment.

To further analyze in detail the effect of DHR and RR building facades on the thermal environment, in addition to the three thermal-environment indicators ( $T_a$ , WBGT, and SET\*), this study measured and evaluated two outdoor radiation-environment indicators (SAT and COT) near the facades using an actual facade-model experiment.

The knowledge obtained from the CFD analysis and actual facade-model experiment is summarized as follows.

- Both the CFD analysis and facade-model experiment demonstrated that the different reflective directional building facades (DHR and RR) have little effect on outdoor *Ta*. However, our study showed that the RR facade could contribute the reduction in the WBGT and SET\* outdoor thermal-environment indicators, compared with the DHR facades.
- The facade-model experiment indicated that the RR facade could reduce the SAT and COT outdoor radiation-environment indicators that mainly considered the effect of short-wave solar-radiation reflection and long-wave radiation from building facades owing to the special reflective directional property of RR materials.
- RR building facades with the same solar reflectance as the DHR facades could effectively reduce the outdoor thermal- and radiation-environment indicators (WBGT, SET\*, SAT, and COT). Thus, they are considered to potentially improve the outdoor environment and minimize the UHI phenomenon.

Our future work will focus on using CFD simulation and actual experiment measurement to profoundly evaluate the effects of RR materials on the ventilation (airflow) environment and air quality around an urban canyon. In addition, from a long-term goal, future work will also focus on the proposals and development of low-cost and high-performance RR materials that can be widely used on the exterior wall surface of buildings.

### Declaration of competing interest

The authors declare that they have no known competing financial interests or personal relationships that could have appeared to influence the work reported in this paper.

### Acknowledgments

This work was supported by “The Obayashi Foundation, Japan (2021)” and “The Hibi Science Foundation, Japan (2021)”. In addition, the authors are sincerely grateful to Mr. Haruto Kitakaze (Master degree in Engineering from Osaka University in March 2020) for his cooperation of conducting CFD analysis of this study.

### References

- [1] W.D. Solecki, C. Rosenzweig, L. Parshall, G. Pope, M. Clark, J. Cox, M. Wiencke, Mitigation of the heat island effect in urban New Jersey, *Global Environ. Change B Environ. Hazards* 6 (1) (2005) 39–49.
- [2] United States Environmental Protection Agency, Reducing Urban Heat Islands: Compendium of Strategies (Report), vols. 7–12, 2008. Available at: <https://www.epa.gov/heatislands/heat-island-compendium>.
- [3] M. Santamouris (Ed.), Energy and Climate in the Urban Built Environment, James and James Science Publishers, London, 2001, <https://doi.org/10.4324/9781315073774>. Available at:
- [4] G. Manoli, S. Fatici, M. Schläpfer, et al., Magnitude of urban heat islands largely explained by climate and population, *Nature* 573 (2019) 55–60.
- [5] Y. Li, X. Zhao, An empirical study of the impact of human activity on long-term temperature change in China: a perspective from energy consumption, *J. Geophys. Res.* 117 (D17) (2012) D17117.
- [6] I. Livada, M. Santamouris, K. Niachou, N. Papanikolaou, G. Mihalakakou, Determination of places in the great Athens area where the heat island effect is observed, *J. Theor. Appl. Climatol.* 71 (2002) 219–230.
- [7] M.L. Imhof, P. Zhang, R.E. Wolfe, L. Bouyou, Remote sensing of the urban heat island effect across biomes in the continental USA, *Remote Sens. Environ.* 114 (2010) 504–513.
- [8] B. Zhou, D. Rybski, J.P. Kopp, On the statistics of urban heat island intensity, *Geophys. Res. Lett.* 40 (2013) 5486–5491.
- [9] W. Liao, et al., Stronger contributions of urbanization to heat wave trends in wet climates, *Geophys. Res. Lett.* 45 (2018) 11310–11317.
- [10] S. Kato, Y. Yamaguchi, Analysis of urban heat-island effect using ASTER and ETM+ Data: separation of anthropogenic heat discharge and natural heat radiation from sensible heat flux, *Rem. Sens. Environ.* 99 (1–2) (2005) 44–54.
- [11] M. Santamouris, Cooling the cities—A review of reflective and green roof mitigation technologies to fight heat island and improve comfort in urban environments, *Sol. Energy* 103 (2014) 682–703.
- [12] H. Akbari, C. Cartalis, D. Kolokotsa, A. Muscio, A.L. Pisello, F. Rossi, M. Santamouris, A. Synnefa, N.H. Wong, M. Zinzi, Local climate change and urban heat island mitigation techniques—the state of the art, *J. Civ. Eng. Manag.* 22 (1) (2016) 1–16.
- [13] J. Yuan, K. Emura, C. Farnham, H. Sakai, Application of glass beads as retro-reflective facades for urban heat island mitigation: experimental investigation and simulation analysis, *Build. Environ.* 105 (2016) 140–152.
- [14] H. Akbari, A.G. Toucheai, Modeling and labeling heterogeneous directional reflective roofing materials, *Sol. Energy Mater. Sol. Cells* 124 (2014) 192–210.
- [15] L. Doulous, M. Santamouris, I. Livada, Passive cooling of outdoor urban spaces. The role of materials, *Sol. Energy* 77 (2) (2004) 231–249.
- [16] E.S. Cozza, M. Alloisio, A. Comite, G. Di Tanna, S. Vicini, NIR-reflecting properties of new paints for energy-efficient buildings, *Sol. Energy* 116 (2015) 108–116.
- [17] S.E. Bretz, H. Akbari, Long-term performance of high-albedo roof coatings, *Energy Build.* 25 (2) (1997) 159–167.
- [18] J. Yuan, K. Emura, H. Sakai, Evaluation of the solar reflectance of highly reflective roofing sheets installed on roofs, *J. Build. Phys.* 37 (2) (2012) 170–184.
- [19] Y. Qin, J. Liang, K. Tan, F. Li, A side by side comparison of the cooling effect of building blocks with retro-reflective and diffuse-reflective walls, *Sol. Energy* 133 (2016) 172–179.
- [20] F. Rossi, B. Castellani, A. Presciutti, E. Morini, M. Filippone, A. Nicolini, M. Santamouris, Retroreflective façades for urban heat island mitigation: experimental investigation and energy evaluations, *Appl. Energy* 145 (2015) 8–20.
- [21] J. Yuan, K. Emura, H. Sakai, C. Farnham, S. Lu, Optical analysis of glass bead retro-reflective materials for urban heat island mitigation, *Sol. Energy* 132 (2016) 203–213.
- [22] R. Levinson, S. Chen, J. Slack, H. Goudey, T. Harima, P. Berdahl, Design, characterization, and fabrication of solar-retroreflective cool-wall materials, *Sol. Energy Mater. Sol. Cell.* 206 (2020) 110117.
- [23] B. Castellani, E. Morini, E. Anderini, M. Filippone, F. Rossi, Development and characterization of retro-reflective colored tiles for advanced building skins, *Energy Build.* 154 (2017) 513–522.
- [24] M. Ichinose, T. Inoue, T. Nagahama, Effect of retro-reflecting transparent window on anthropogenic urban heat balance, *Energy Build.* 157 (2017) 157–165.
- [25] J. Yuan, C. Farnham, K. Emura, Evaluation of retro-reflective properties and upward to downward reflection ratio of glass bead retro-reflective material using a numerical model, *Urban Clim.* 36 (2021) 100774, <https://doi.org/10.1016/j.ulclim.2021.100774>.
- [26] F. Rossi, A.L. Pisello, A. Nicolini, M. Filippone, M. Palombo, Analysis of retro-reflective surfaces for urban heat island mitigation: a new analytical model, *Appl. Energy* 114 (2014) 621–631.
- [27] B. Castellani, A. Nicolini, A.M. Gambelli, M. Filippone, E. Morini, F. Rossi, Experimental assessment of the combined effect of retroreflective facades and pavement in urban canyons, *IOP Conf. Ser. Mater. Sci. Eng.* 609 (2019), 072004. <https://doi:10.1088/1757-899X/609/7/072004>.
- [28] J. Yuan, C. Farnham, K. Emura, Geometrical-optics analysis of reflective glass beads applied to building coatings, *Sol. Energy* 122 (2015) 997–1010.
- [29] G. Lobaccaro, J. Acero, G. Martinez, A. Padro, T. Laburu, G. Fernandez, Effects of orientations, aspect ratios, pavement materials and vegetation elements on thermal stress inside typical urban canyons, *Int. J. Environ. Res. Publ. Health* 16 (2019) 3574.
- [30] J. Yuan, K. Emura, C. Farnham, Is urban albedo or urban greening covering more effective for urban microclimate improvement? : A simulation for Osaka, *Sustain. Cities Soc.* 32 (2017) 78–86.
- [31] H. Takebayashi, M. Moriyama, K. Miyake, Analysis on the relationship between properties of urban block and wind path in the street canyon for the use of the wind as the climate resources, *J. Environ. Eng.* 635 (2009) 77–82 (In Japanese).
- [32] H. Kitakaze, J. Yuan, T. Yamanaka, T. Kobayashi, Influence of building envelope's solar Reflectivity, Wind speed and building coverage ratio on urban heat environment, in: The 40th AIVC - 8th Tight Vent & 6th Ventcool Conference, 2019, pp. 365–374.
- [33] Ministry of Land, Infrastructure, Transport and Tourism of Japan: evaluation tool for thermal environment measures in cities (in Japanese), [http://www.env.go.jp/air/life/heat\\_island/guidelineH30/07\\_chapter5\\_6.pdf](http://www.env.go.jp/air/life/heat_island/guidelineH30/07_chapter5_6.pdf).
- [34] M. Ono, M. Tonouchi, Estimation of wet-bulb globe temperature using generally measured meteorological indices, *Jpn. J. Biometeorol.* 50 (4) (2014) 147–157 (in Japanese).
- [35] International Organization for Standardization, ISO 7243. Hot Environments - Estimation of the Heat Stress on Working Man, Based on the WBGT-Index, Wet Bulb Globe Temperature, 1989.
- [36] J. Pickup, R. De Daer, An outdoor thermal comfort index (OUT\_SET\*) - part I -the model and its assumptions, in: 15th International Congress of Biometereology and International Conference on Urban Climatology 83, 1999.
- [37] Japanese Industrial Standards Committee, Determination of reflectance of solar radiation by paint film, JIS K5602: 2008 (in Japanese), <https://kikakurui.com/k5/K5602-2008-01.html>.
- [38] Japan Testing Center for Construction Materials (JTCCM), How to Measure the Radiant Air Temperature of the Building Peripheral Wall with a SAT Meter, JSTM J 6110: 2003 (in Japanese), <https://www.jtccm.or.jp/publication/tqid/721/Default.aspx>.
- [39] K. Kohri, H. Ishino, T. Furukawa, A study on evaluation of radiant effect from each surface in atria through field measurement, *J. Archit. Plann. Environ. Eng., AJI* 535 (2000) 9–14 (in Japanese).
- [40] B. Castellani, A.M. Gambelli, A. Nicolini, F. Rossi, Optic-energy and visual comfort analysis of retro-reflective building plasters, *Build. Environ.* 174 (2020) 106781.
- [41] S. Fujita, T. Inoue, M. Ichinose, T. Nagahama, S. Takakusa, Improvement of outdoor radiative environment by high-reflective façade – effect of heat-shielding

- film with retro-reflective property in near infrared band-, *J. Environ. Eng., AJJ* 79 (696) (2014) 167–172 (in Japanese).
- [42] S. Cocco, J. Kämpf, J.L. Scartezzini, D. Pearlmuter, Outdoor human comfort and thermal stress: a comprehensive review on models and standards, *Urban Clim.* 18 (2016) 33–57.
- [43] A. Sharma, P. Conry, H.J.S. Fernando, A.F. Hamlet, J.J. Hellmann, F. Chen, Green and cool roofs to mitigate urban heat island effects in the Chicago metropolitan area: evaluation with a regional climate model, *Environ. Res. Lett.* 11 (2016), 064004.
- [44] S.A. Epstein, S.M. Lee, A.S. Katzenstein, M. Carreras-Sospedra, X. Zhang, S. C. Farina, et al., Air-quality implications of widespread adoption of cool roofs on ozone and particulate matter in southern California, *Proc. Natl. Acad. Sci. U.S.A.* 114 (34) (2017) 8991–8996.